Genetic basis of downy mildew resistance in cucumber: Identification of candidate genes and ethylene-mediated defense mechanism

Mahdi Badri Anarjan
Chunying Zhang
Shahida Begum
Khin Thanda Win
Haisu Li
Chunhua Wang
Tao Wu
Sanghyeob Lee

sanglee@sejong.ac.kr

Sejong University https://orcid.org/0000-0001-7684-2325

Research Article

Keywords: 1-aminocyclopropane-1-carboxylate oxidase, Carbonic anhydrase, Downy mildew, Ethylene, Serine/threonine-protein kinase

Posted Date: July 10th, 2025

DOI: https://doi.org/10.21203/rs.3.rs-6706016/v1

Abstract

The present study aimed to reveal the the genetic factors underlying downy mildew (DM) resistance in cucumber. We established three mapping populations, including two recombinant inbred lines (dm2.1-F_7 and dm2.2-F_7) and one near isogenic line (dm5.1-BC_4F_2), all derived from the cross between TH118FLM (DM-resistant) and WMEJ (DM-susceptible). These lines exhibited a skewed susceptibility distribution, suggesting the involvement of crucial recessive genes in DM-resistance. A quantitative trait locus (QTL)-seq analysis of the pooled populations of these lines effectively refined the genomic regions of *dm2.1*, *dm2.2*, and *dm5.1*. Subsequent single-nucleotide polymorphism mining further refined these regions and identified candidate genes, with *dm2.1*, *dm2.2*, and *dm5.1* spanning 61.7, 84.7, and 80 Kb and encompassing 7, 10, and 5 putative genes, respectively. Finally, *CsaV3_2G012920* (*CsACO*, 1-aminocyclopropane-1-carboxylate oxidase), *CsaV3_2G030320* (*CsCA*, carbonic anhydrase), and *CsaV3_5G015170* (*CsSTPK*, serine/threonine-protein kinase) were identified as candidate DM-resistance genes, based on sequence and expression differences between DM-resistant and DM-susceptible lines. Furthermore, *in silico* 3D modeling revealed structural variations in *CsaV3_5G015170* but not *CsaV3_2G012920* and *CsaV3_2G030320*. Based on the presumed functions and transcriptional responses of these genes to ethephon treatment, we proposed an ethylene-mediated defense mechanism for DM-resistance. According to this model, *Pseudoperonospora cubensis* first induces *CsACO* expression, leading to ethylene production, and then induces *CsCA* and *CsSTPK* expression, resulting in stomatal closure preventing pathogenic hyphal penetration and ethylene-mediated signaling pathway activation, respectively. These findings enhance our understanding of the genetic mechanisms underlying DM-resistance in cucumbers and further support our efforts to combat this destructive disease.

Introduction

Cucumber, a member of the *Cucurbitaceae* family, belongs to the *Cucumis* genus (Sikdar et al. 2010). The *Cucumis* genus comprises cultivated species, such as *Cucumis sativus* var. *sativus* (cucumber), and *Cucumis melo* (melon), along with several wild species, including *Cucumis sativus* var. *hardwickii*, *Cucumis hystrix*, and *Cucumis callosus* (Weng 2010; Kacar et al. 2012; Lv et al. 2012; Qi et al. 2013; Badri Anarjan et al. 2024).

In cucumber production, challenges arise because of the presence of both pre- and post-harvest diseases (St. Amand and Wehner 1991; Badri Anarjan et al. 2021; Badri Anarjan et al. 2022). Cucumbers are susceptible to a wide range of diseases and pests throughout their growth cycle. Among these, downy mildew (DM) is a common foliar diseases, caused by the obligate biotrophic oomycete pathogen *Pseudoperonospora cubensis* (Call et al. 2012a, b; Cohen et al. 2014). To manage and prevent DM in cucumbers, various approaches have been proposed, including environmental control, fungicide application, and biotechnological methods (Ojiambo et al. 2015). However, implementing environmental control and fungicide applications in cucumber cultivation fields is often impractical because of certain limitations. Therefore, there is an urgent need to develop cucumber cultivars that are resistant to DM.

Studying the genetic inheritance of DM-resistance, identifying DM-resistance gene(s), and incorporating DM-resistant germplasms in cucumber breeding programs have been considered the most cost-effective approaches to control DM (Cohen et al. 2015; Wallace et al. 2015).

The search for DM-resistance in cucumber germplasm began in 1942 and has persisted for several decades (Jenkins 1942). In 1954, a plant introduction line, designated PI197087, displayed resistance to DM (Barnes and Epps 1954). This resistance was attributed to a recessive resistance gene called *dm-1*. Following this discovery, several DM-resistant cucumber varieties, such as Gy4, Chipper, and the Marketmore series, were developed through the introgression of the *dm-1* gene (Wehner and Shetty 1997; Call et al. 2012a).

However, in 2004, a significant challenge arose with the emergence of new strain(s) of *P. cubensis*, capable of overcoming the resistance conferred by *dm-1*. This development led to widespread damage in cucumber production in the United States (Holmes et al. 2015). Since then, extensive research has been dedicated to identifying cucumber germplasms resistant to these new *P. cubensis* strains. This led to the identification of three DM-resistant cucumber collections, namely PI197088, PI330628, and PI605996 (Call et al. 2012b). Notably, PI197088 has been the focus of extensive investigation, resulting in the successful identification of several quantitative trait loci (QTLs) associated with DM-resistance in this germplasm (Yoshioka et al. 2014; Li et al. 2018; Wang et al. 2018). Additionally, PI330628-originated DM-resistance revealed the presence of four QTLs located on cucumber chromosomes 2, 4, 5, and 6 (Wang et al. 2016). Furthermore, a North China-type cucumber line, K8, was found to have five DM-resistance QTLs, namely *dm1.1*, *dm5.1*, *dm5.2*, *dm5.3*, and *dm6.1*, distributed across three different chromosomes (Zhang et al. 2013). Another DM-resistant germplasm, IL52, harbors six QTLs (Pang et al. 2013). Moreover, PI 197085-originated DM-resistance was found to be controlled by a QTL locus on chromosome 5 (Szczechura et al. 2015). The Korean inbred line TH118FLM displays DM-resistance through six QTLs: *dm2.1*, *dm2.2*, *dm4.1*, *dm5.1*, *dm5.2*, and *dm6.1* (Win et al. 2017).

Although numerous QTLs associated with DM-resistance have been identified, their integration into marker-assisted breeding (MAB) programs remains a challenge. The process of identifying DM-resistance genes within these QTLs requires the application of fine-mapping technologies. However, the fine mapping of these large QTLs has proven to be a formidable task, and only a limited number of QTLs have been successfully subjected to fine mapping (Pan et al. 2018; Wang et al. 2019; Berg et al. 2020, 2021). Considering the complex genetic inheritance underlying DM-resistance, the fine mapping of DM-resistance QTLs presents significant challenges. Notably, the first DM-resistance gene in PI197087, *dm1*, was successfully identified as the *STAY-GREEN* (*CsSGR*) gene in the Gy14 cucumber variety developed from the same germplasm (Wang et al. 2019). The QTL *dm4.1* in PI197088 was ultimately mapped into sub-QTLs *dm4.1.1*, *dm4.1.2*, and *dm4.1.3*, among which *dm4.1.2* and *dm4.1.3* were regulated by a *receptor-like kinase* (*CsLRK*) gene and an *amino acid permease 2A* (*CsAPP2A*) gene, respectively (Berg et al. 2020, 2021). Subsequently, the *CsSIB1* gene encoding sigma factor binding protein 1 emerged as the top candidate for the *dm5.3* locus in PI197088 (Tan et al. 2022).

In our previous study, we identified three major QTLs associated with DM-resistance located on chromosomes 2 and 5 (Win et al. 2017), namely *dm2.1*, *dm2.2*, and *dm5.1*, spanning genomic regions from 6.68 to 10.87 Mb, 19.08 to 21.02 Mb, and 6.73 to 15.24 Mb, respectively. To fine-genetic mapping and identify the candidate gene(s) within these DM-resistance QTLs, we implemented a two-step approach. First, we established mapping populations based on near-isogenic lines (NILs) and recombinant inbred lines (RILs), followed by the application of bulk segregant analysis (BSA)-assisted QTL-seq and single nucleotide polymorphism (SNP)-mining analysis to identify sub-QTLs. Through this method, we successfully narrowed down and fine-mapped *dm2.1*, *dm2.2*, and *dm5.1* to remarkably compact genomic regions of sizes 61.7, 84.7, and 80.0 Kb, respectively. Subsequently, our expression analysis led to the identification of *CsaV3_2G012920* (1-aminocyclopropane-1-carboxylate oxidase), *CsaV3_2G030320* (carbonic anhydrase), and *CsaV3_5G015170* (serine/threonine-protein kinase) as the genes underlying DM-resistance within QTLs *dm2.1*, *dm2.2*, and *dm5.1*, respectively. Moreover, compelling evidence suggests that DM-resistance may be acquired through the ethylene-mediated signaling pathway involving these three candidate genes. These findings significantly advance our understanding of the molecular mechanisms underlying DM-resistance in cucumbers and contribute to our efforts to combat this destructive disease.

Materials and methods

Development of mapping populations and plant growth conditions

Two populations of RILs, named dm2.1-F_7 for *dm2.1* and dm2.2-F_7 for *dm2.2* QTL loci, as well as a NIL population, dm5.1-BC_4F_2 for *dm5.1* QTL locus were used in this study. These populations were derived from two parental inbred lines, namely TH118FLM (DM-R), a self-pollinating inbred line derived from the commercial hybrid variety 'Malini' (Monsanto), and WMEJ (DM-S), obtained from a Korean hybrid cucumber ‘Joeun’. These populations were developed in the greenhouses of the Asia Seed Company (Icheon, South Korea) using the method depicted in Supplementary Fig. 1 between 2013 and 2019. In our marker-assisted selection (MAS) of the RIL and NIL populations, we employed various types of markers, including simple-sequence repeat (SSR), insertion/deletion (InDel), and cleaved amplified polymorphic sequence (CAPS) markers. In this approach, we used eight markers to study each QTL: *dm2.1* (three InDel, four CAPS, and one SSR), *dm2.2* (three InDel, two CAPS, and three SSRs), and *dm5.1* (two InDel, three CAPS, and three SSRs) (Fig. 2b, Fig. 3b, Fig. 4b, Supplementary Table 1). Those markers enough cover the previous identified three major QTL loci (*dm2.1*, *dm2.2*, and *dm5.1*) associated with DM-resistance located on chromosomes 2 and 5 by Win et al. (2017). In order to fine-genetic mapping of three major QTL loci via QTL-seq and single nucleotide polymorphism (SNP)-mining analysis, during the summers of 2019 and 2020, we cultivated a set of 100, 131, and 146 individuals for the dm2.1-F_7, dm2.2-F_7, and dm5.1-BC_4F_2 populations, respectively, in the greenhouse facilities of the Asia Seed Company. All plants were cultivated in peat bags and drip-irrigated with a nutrient solution. Throughout the growth

period, appropriate plant protection measures were implemented to ensure their well-being and protection against potential threats or diseases.

Table 2
Downy mildew resistance (DM-R) QTLs in the cucumber inbred line TH118FLM

QTL	Chr.	Source of resistant allele	Physical position [a]		
			Original [b]	QTL-seq analysis	SNP-mining approach
dm2.1	2	DM-R	6.68–10.87 (4.19 Mb)	10,384,014 – 10,717,274 (333,260 bp)	10,461,069 – 10,522,788 (61,719 bp)
dm2.2	2	DM-R	19.08–21.02 (1.94 Mb)	19,675,000–19,971,200 (296,200 bp)	19,833,180 – 19,917,905 (84,725 bp)
dm5.1	5	DM-R	6.73–15.24 (8.51 Mb)	11,854,372 – 12,548,640 (694,268 bp)	12,351,644 – 12,431,634 (79,990 bp)

a) Physical positions of the corresponding QTLs are on the cucumber reference genome (*Cucumis sativus* L. var. *sativus* cv. Chinese Long v3). b) The physical position of three major-effect QTL loci for DM-resistance are obtained from Win et al. (2017).

Evaluation of disease index (DI)

During the summers of 2019 and 2020, we conducted greenhouse screenings to assess the symptoms of DM-disease in two parentally inbred lines, as well as in their RIL and NIL populations. Under controlled greenhouse conditions, the onset of naturally occurring DM-disease became evident approximately 60 days after planting. During this stage, DM-disease symptoms became apparent and distinguishable. The disease continued to progress for approximately two weeks, during which the symptoms extended to all parts of the affected plants. Following the approach described by Pang et al. (2013), the phenotypes were assigned a score on a scale of 1 (no symptoms) to 8 (maximum symptoms) (Fig. 1a). The DI of the three populations was evaluated using three separate assessments during each growth session. The average DI derived from these six evaluations was computed to determine the mean DI for each individual in the population (Fig. 1b-d).

Generation of DM-R and DM-S bulks

Two bulks, consisting of individuals exhibiting extreme resistance and susceptibility to DM, were assembled for whole-genome re-sequencing. For the dm2.1-F_7, dm2.2-F_7, and dm5.1-BC_4F_2 populations, the DM-R bulk was formed by selecting six, nine, and eight lines, respectively that consistently exhibited

extreme resistance to DM (Fig. 1b-d, Supplementary Table 2). In addition, the DM-S bulk was formed by selecting 11 lines each, from the three populations, that consistently exhibited extreme susceptibility to DM (Fig. 1b-d, Supplementary Table 2).

Isolation of genomic DNA (gDNA) and whole-genome re-sequencing

The gDNA was extracted following the procedure outlined by Zhang et al. (2021). To create bulk DM-R and DM-S, equimolar quantities of gDNA from each individual within the respective bulk were pooled and thoroughly mixed. Library construction (280-bp insert size) for sequencing was performed by Clinomics Inc. (Seoul, Korea). Sequencing was performed in a paired-end configuration (2 × 100 bp) using an Illumina HiSeq 2000 sequencer (Illumina, San Diego, CA, USA). HiSeq Sequencing Kits (Illumina) were employed to ensure accurate and efficient sequencing of the samples. Raw paired-end reads were generated using a base-calling pipeline that utilized the sequencing control software (SCS) provided by Illumina. This pipeline facilitates the conversion of the raw sequencing data into readable nucleotide sequences, serving as the foundation for subsequent downstream analysis and interpretation.

QTL-seq analysis by bulked segregant analysis

We employed the BSA-assisted QTL-seq method, following the procedure outlined by Zhang et al. (2021). The key aspects of this method are summarized here. We considered SNPs with a SNP-index less than 0.3 in one bulk and 0.3 or greater in the other bulk as authentic SNPs. When the DM-S short reads contained an SNP, they were assigned an SNP index value of 0, whereas the DM-R short reads harboring an SNP were assigned an SNP index value of 1. The differences between SNP indices were calculated as follows: Δ (SNP-index) = SNP-index (DM-R) − SNP-index (DM-S). To compute the average SNP-index, we used a sliding-window approach with a window size of 2 Mb and an increment of 10 kb for each genomic interval. To ensure the accuracy of QTL identification via QTL-seq, we determined the statistical confidence intervals for Δ (SNP-index) under the null hypothesis of no QTLs, following the methodology described by Takagi et al. (2013).

SNP-mining approach for fine-genetic mapping

SNP-mining was employed to identify specific and compact regions within the loci initially identified through QTL-seq analysis. For this, we used Geneious Pro 9.1.8 (Biomatters, Auckland, New Zealand), adhering to the manufacturer's guidelines. We imported all sequences from the two parental lines (DM-R and DM-S) and the DM-R and DM-S bulks corresponding to the regions associated with *dm2.1*, *dm2.2*, and *dm5.1* into Geneious Pro 9.1.8. Subsequently, we extracted all SNPs and InDels that showed identical matches within the short reads of either DM-R or DM-S. Similarly, we isolated all SNPs and InDels that showed perfect identity within the short reads of either the DM-R or DM-S bulks. Thereafter, a comparative analysis of these SNPs and InDels enabled us to identify regions where sequence variations

between the parental lines were completely conserved in both bulks, without any exceptions. This approach enabled us to narrow down the regions associated with *dm2.1*, *dm2.2*, and *dm5.1*.

P. cubensis inoculation and ETH treatment

Both the DM-R and DM-S lines were cultivated in a growth chamber (Daihan Scientific, Wonju, South Korea) under long-day conditions (16/8-hour light/dark photoperiod) at a temperature of 23°C and a light intensity of 120 μmol m^{-2} s^{-1}. To obtain *P. cubensis* conidia for inoculation, spores were collected from the leaves of naturally infected DM-S plants in a greenhouse. The spores were washed from the infected leaves using tap water and subsequently filtered through cheesecloth (Thermo Fisher Scientific, Rochester, NY, USA). The spore suspension was adjusted to 1×10^4 spores/mL using 0.01% Tween-20 (Sigma-Aldrich). The DM-spore suspension was sprayed onto the leaves of seedlings at the two-true-leaf stage. After inoculation, polythene sheets (CleanLab, Seoul, Korea) were placed on cucumbers to maintain optimal humidity levels. By the 7 dpi, *P. cubensis* spores exhibited yellowing, indicating the presence of the DM-disease. For the ETH (Sigma-Aldrich, MO, USA) treatment, a 100 ppm ETH solution was prepared using ethyl alcohol (Sigma-Aldrich) and applied by spraying it onto the leaves of seedlings at the two-true-leaf stage.

Total RNA isolation and expression analysis

To analyze the expression of the DM-resistance candidate genes *CsaV3_2G012920*, *CsaV3_2G030320*, and *CsaV3_5G015170*, we sampled five leaves from each plant at both 0 and 3 dpi. For evaluating the ETH treatment of these candidate genes, leaves were collected at 0, 6, 12, and 24 hpi. Following immediate collection, the samples were promptly flash-frozen in liquid nitrogen and stored at -80°C. Subsequently, total RNA was extracted and reverse transcription-polymerase chain reaction (RT-PCR) was performed according to the protocols of Zhang et al. (2021). For RT-PCR three forward- and reverse primer sets were used (Supplementary Table 3). This process was repeated three times.

Observation of stomatal opening and closure

Leaf samples treated with 100 ppm ETH were collected at eight hpi. The leaf epidermal layers were gently removed using a razor, and the stomata of the leaf samples were then examined under a LEICA DMi8 microscope (Wetzlar, Germany) at 400X magnification.

Measurement of stomatal conductance

The fourth true leaves of both DM-R and DM-S plants were relocated to the greenhouse of Gyeongsang National University (Jinju, Gyeongsangnam-do, South Korea) two days prior to measurement. These plants were positioned under a light intensity of 200 μmol m^{-2} s^{-1} and received ample watering to prevent water stress during the assessment. In order to observe the impact of ETH on stomatal

conductance, all plants were treated with either 100 ppm of ETH or a control solution (0 ppm). The measurements commenced at 2 PM on December 7, 2023, within the greenhouse environment. Measurements were taken at 0, 2, 4, 6, and 21 hours post-treatment using the center of the fourth true leaf and an LI-600 Porometer/Fluorometer (LI-COR, Lincoln, NE, USA). Each measurement was conducted in triplicate using three plants for both the control and ETH treatment groups.

In silico 3D modeling and comparison of protein structures

We utilized the amino acid sequences from both DM-R and DM-S for the three DM-resistance candidate genes. To predict their 3D structures, we employed SWISS-MODEL (https://swissmodel.expasy.org), using the default parameter settings, as detailed Waterhouse et al. (2018). Subsequently, we imported the 3D protein structures in the form of PDB (Protein Data Bank) files into Geneious Pro 9.1.8. The visualization, comparison, and alignment of these 3D protein structures were performed in accordance with established procedures using Geneious Pro 9.1.8.

Statistical analysis

All measurements were derived from at least three biological samples. To ascertain the presence of significant differences, all statistical analyses were conducted using MATLAB (R2020a, The MathWorks, Natick, MA, USA). Statistical significance was established with a threshold set at a $P < 0.05$.

Results

Genetic inheritance of DM-resistance

Two sets of parentally inbred lines, TH118FLM (DM-R) and WMEJ (DM-S), were used to generate the mapping populations for fine-genetic mapping of three major QTL loci via QTL-seq and SNP-mining analysis (Supplementary Fig. 1). DM-R displayed no signs of DM-disease symptoms, with a disease index (DI) of 1, whereas DM-S exhibited severe symptoms, with a DI of 8 (Fig. 1a). This study involved the establishment of two RIL mapping populations, dm2.1-F_7 (comprising 100 individuals) and dm2.2-F_7 (comprising 131 individuals), along with a NIL mapping population, dm5.1-BC_4F_2 (comprising 146 individuals). The DI distribution across the mapped populations ranged from 1 to 8, displaying an asymmetric trend with a noticeable inclination towards a susceptible phenotype (Fig. 1b-d). This suggests that a limited number of crucial recessive genes (s) exerted a substantial influence on DM-resistance within these populations, holding promise for subsequent QTL mapping to uncover and comprehend the genetic foundation of DM-resistance.

Whole-genome re-sequencing

In our previous study (Win et al. 2017), we sequenced the genomes of the parental lines DM-R (SRR4159531) and DM-S (SRR4159532). For this, three sets each of DM-resistant (R-bulks) and DM-susceptible bulks (S-bulks) from the dm2.1-F_7, dm2.2-F_7, and dm5.1-BC_4F_2 lines were subjected to re-sequencing.

A total of 90.2, 89.4, and 89.5 million filtered reads were produced from the R-bulks of dm2.1-F_7, dm2.2-F_7, and dm5.1-BC_4F_2 lines, respectively (Table 1). Of these, 88.7 (dm2.1-F_7-R-bulk), 87.9 (dm2.2-F_7-R-bulk), and 87.7 million (dm5.1-BC_4F_2-R-bulk) filtered reads aligned to the reference genome. Each of these sequences exhibited a genome coverage of 99.69%, 99.67%, and 99.39%, respectively. Similarly, the S-bulks of dm2.1-F_7, dm2.2-F_7, and dm5.1-BC_4F_2 lines generated a total of 89.9, 90.0, and 90.3 million filtered reads, with respective genome coverages of 99.68%, 99.22%, and 99.93% (Table 1). All sequences were submitted to the Sequence Read Archive (SRA) database of the National Center for Biotechnology Information (NCBI) (https://www.ncbi.nlm.nih.gov/sra/term=) and can be accessed using the following IDs: dm2.1-F_7-R-bulk (SRR26038220), dm2.1-F_7-S-bulk (SRR26038219), dm2.2-F_7-R-bulk (SRR26038218), dm2.2-F_7-S-bulk (SRR26038217), dm5.1-BC_4F_2-R-bulk (SRR26038216), and dm5.1-BC_4F_2-S-bulk (SRR26038215).

Table 1
Statistical analysis of sequencing results and unique read coverage of the cucumber genome

Sample	No. of raw reads	No. of filtered reads (%)[a]	No. of aligned reads (%)[b]	Genome coverage (%)[c]
DM-R[d]	109,977,506	103,204,050 (93.84)	94,519,285 (91.58)	97.94
DM-S[d]	132,215,510	126,026,876 (95.31)	114,219,265 (90.63)	99.50
dm2.1-F_7-R-Bulk	90,490,326	90,200,632 (99.67)	88,676,241 (98.31)	99.69
dm2.1-F_7-S-Bulk	90,224,706	89,957,836 (99.70)	88,401,565 (98.27)	99.68
dm2.2-F_7-R-Bulk	89,644,730	89,427,654 (99.75)	87,889,498 (98.28)	99.67
dm2.2-F_7-S-Bulk	90,312,654	90,043,014 (99.70)	88,143,106 (97.89)	99.22
dm5.1-BC_4F_2-R-Bulk	89,704,742	89,457,886 (99.72)	87,668,728 (98.13)	99.39
dm5.1-BC_4F_2-S-Bulk	90,637,488	90,372,830 (99.70)	87,661,645 (97.51)	99.93

a) Percentage represents the ratio of number of filtered reads from number of raw reads. b) Percentage represents the ratio of number of aligned reads to the cucumber *Cucumis sativus* L. var. *sativus* cv. Chinese Long v3 sequence from number of raw reads. c) *Cucumis sativus* L. var. *sativus* cv. Chinese Long v3 was used as a cucumber reference genome sequence. d) The sequences were downloaded from the NCBI-SRA database under the IDs of SRR4159531 (DM-R) and SRR4159532 (DM-S).

Refining of DM-resistance QTLs by NIL- and RIL-mediated QTL-seq analysis

We previously identified three genomic regions, *dm2.1* (6.68–10.87 Mb on chromosome 2), *dm2.2* (19.08–21.02 Mb on chromosome 2), and *dm5.1* (6.73–15.24 Mb on chromosome 5), associated with DM-resistance in the TH118FLM cucumber line (Fig. 2a, Fig. 3a, Fig. 4a, Table 2). However, despite these findings, the exact genes responsible DM-resistance in these regions remained unclear because of their large genomic spans. To further elucidate the genes underlying these DM-resistance regions, we used BSA-assisted QTL-seq. This involved using two populations for mapping NILs and RILs and using the DM-S line as the reference genome.

Analysis of the Δ (SNP-index) plots allowed us to narrow down the genomic segments of *dm2.1*, *dm2-2*, and *dm5.1*. Notably, *dm2.1* was located within a 333-kb genomic region spanning from 10.38 to 10.72 Mb (Fig. 2b, Fig. 5a, Supplementary Fig. 2a-c, Table 2). This region exhibited an average single nucleotide polymorphism-index (SNP-index) above 0.9 in the R-bulk, in contrast to a value below 0.1 in the S-bulk. Similarly, *dm2.2* was mapped within a 296-kb genomic region between 19.68 and 19.97 Mb (Fig. 3b, Fig. 5b, Supplementary Fig. 3a-c, Table 2). The SNP-index pattern in this region corresponded with the DM-resistance trend observed in *dm2.1*. Likewise, *dm5.1* was localized to a 694-kb genomic region extending from 11.85 Mb to 12.55 Mb (Fig. 4b, Fig. 5c, Supplementary Fig. 4a-c, Table 2), exhibiting SNP-index characteristics consistent with DM-resistance, as observed in previous cases. Upon reference genome annotation (Chinese Long 9930 V3.0), the *dm2.1*, *dm2.2*, and *dm5.1* regions were found to potentially contain 31, 35, and 55 putative genes, respectively. Additional information is provided in Supplementary Table 4 for reference.

Further refining of DM-resistance by single nucleotide polymorphism-mining (SNP-mining) analysis

To achieve more precise mapping of *dm2.1*, *dm2.2*, and *dm5.1*, we employed the SNP-mining technique. As a result, *dm2.1* was further refined to a specific 61.7-Kb interval spanning from 10.46 Mb to 10.52 Mb (Fig. 2c, Table 2, Supplementary Table 4–5). Similarly, the genomic region for *dm2.2* was refined to an 84.7-Kb region spanning from 19.83 Mb to 19.92 Mb (Fig. 3c, Table 2, Supplementary Table 4–5). For *dm5.1*, the genomic region was specifically narrowed down to an 80-Kb interval, extending from 12.35 Mb to 12.43 Mb (Fig. 4c, Table 2, Supplementary Table 4–5). According to reference genome annotation, the refined QTLs *dm2.1*, *dm2.2*, and *dm5.1* contained seven, ten, and five putative genes, respectively (Fig. 2d, Fig. 3d, Fig. 4d, Supplementary Table 4).

Identifying candidate genes associated with DM-resistance within the dm2.1, dm2.2, and dm5.1 loci

We conducted a study to identify the candidate genes responsible for the DM-resistance conferred by *dm2.1*, *dm2.2*, and *dm5.1*. Initially, we focused on identifying genes displaying sequence variations in genic sequences between the DM-R and DM-S lines. In *dm2.1*, we identified four genes

(*CsaV3_2G012900*, *CsaV3_2G012910*, *CsaV3_2G012920*, and *CsaV3_2G012930*) with polymorphic regions between DM-R and DM-S. Among these genes, only *CsaV3_2G012920*, which was predicted to encode 1-aminocyclopropane-1-carboxylate oxidase (ACO), exhibited a non-synonymous mutation, whereas the other three genes harbored synonymous mutations (Supplementary Table 4). In *dm2.2*, a single gene, *CsaV3_2G030320*, potentially encoding carbonic anhydrase (CA), displayed a non-synonymous mutation (Supplementary Table 4). In *dm5.1*, three genes (*CsaV3_5G015160*, *CsaV3_5G015170*, and *CsaV3_5G015190*) showed polymorphisms in the genic region between the DM-R and DM-S groups. Among these three genes, only *CsaV3_5G015170*, which putatively encodes a serine/threonine-protein kinase (STPK), exhibited a non-synonymous mutation, whereas the other two had synonymous mutations (Supplementary Table 4).

Subsequently, we examined the expression of the three identified genes. *CsaV3_2G012920* and *CsaV3_2G030320* showed increased mRNA transcript levels in DM-resistant plants within 3 days post inoculation (dpi) (Figs. 6A, B). Conversely, *CsaV3_5G015170* showed relatively suppressed mRNA transcript levels in DM-resistant plants compared to DM-susceptible plants, despite both groups inducing mRNA transcription within 3 dpi (Fig. 6c).

Expression of the DM-resistance candidate genes and stomatal action in response to ethephon (ETH) treatment

The enzyme 1-aminocyclopropane-1-carboxylate oxidase (ACO) plays a crucial role in ethylene (ET) production (Rudus et al. 2013). Among the genes potentially associated with DM-resistance, one candidate was *CsaV3_2G012920*, which potentially encodes ACO. Therefore, we postulate that ET is involved in cucumber DM-resistance. Initially, we measured their transcript levels to determine whether these three genes could respond to ET through the release of ETH. The results showed that all three genes exhibited increased transcript levels from 6 to 24 h after application (Figs. 7A, B, C). Another DM resistance candidate gene, *CsaV3_2G030320*, encodes carbonic anhydrase (CA), a key regulator of stomatal closure (Majeau et al. 1994). This prompted us to examine how ETH influences stomata action. After applying ETH, a noticeable closure of stomata was observed in the DM-resistance line after 8 h (Supplementary Fig. 5). Additionally, we compared stomatal conductance in DM-resistance and DM-susceptible plants with and without ETH application. In DM-susceptible plants, ETH application did not significantly impact stomatal behavior except at the 6-h mark following application (Figs. 8A, B). Similarly, in DM-resistance plants, ETH application marginally increased stomatal conductance at 4 h. However, after 6 h of ETH application, there was a significant decrease in stomatal conductance in DM-R plants (Figs. 8A, B). These findings strongly indicate that the heightened presence of ETH in DM-resistance plants is adequate to prompt stomatal closure.

In silico 3D modeling of DM-resistance candidate genes

We conducted *in silico* 3D modeling of protein structures for three potential DM-resistance candidate genes, *CsaV3_2G012920*, *CsaV3_2G030320*, and *CsaV3_5G015170*, to identify structural distinctions between DM-resistant and DM-susceptible lines. For *CsaV3_2G012920*, we observed a single non-

synonymous mutation, where isoleucine (I) in the DM-susceptible line was replaced by valine (V) in the DM-resistant line at amino acid position 91 within an α-helix (Supplementary Fig. 6). However, despite the presence of this non-synonymous mutation ($I^{91} \rightarrow V^{91}$), this genetic polymorphism caused no discernible alteration in protein structure. In the case of *CsaV3_2G030320*, four non-synonymous mutations were identified in DM-resistant plants. These mutations included the substitution of phenylalanine (F) with isoleucine (I) at amino acid position 26 within a β-sheet, threonine (T) with isoleucine (I) at amino acid position 165 within an α-helix, glycine (G) with aspartate (D) at amino acid position 194 within a β-sheet, and aspartate (D) with asparagine (N) at amino acid position 287 (Supplementary Fig. 7). Similar to *CsaV3_2G012920*, these changes could not alter the protein structure of the *CsaV3_2G030320* protein. In the case of *CsaV3_5G015170*, a non-synonymous sequence polymorphism was found between the two parental inbred lines (DM-R and DM-S), which led to the mutation of cysteine (C) in DM-S to arginine (A) in DM-R at amino acid position 653 (Supplementary Fig. 8). This non-synonymous mutation occurred within the protein kinase domain, resulting in the formation of an additional β-sheet in DM-resistant lines. Furthermore, significant dissimilarity was observed in the C-terminal structure beyond amino acid 653 between the DM-resistant and DM-susceptible lines.

Discussion

Typical QTL mapping approaches often reveal extensive QTL regions spanning multiple centimorgans (cMs) and encompassing numerous potential genes. This methodology is valuable for identifying chromosomal regions associated with specific traits. However, its practicality in breeding programs is constrained by the challenges involved in effectively incorporating QTL segments, including the target gene, while avoiding undesirable linked genes. Consequently, fine-mapping techniques have been developed to narrow down these QTL regions. The degree of QTL precision depends on various factors such as the type and size of the population, accuracy of phenotyping, and quantity of markers (Dinka et al. 2007; Cobb et al. 2013; Jaganathan et al. 2020).

Recent advancement in sequencing technologies has significantly facilitated the detection of single nucleotide polymorphisms (SNPs) and their utility in high-throughput screening of genetic variations. Next-generation sequencing (NGS)-based mapping tools, including restriction site-associated DNA sequencing (RAD-seq), genotyping-by-sequencing (GBS), whole-genome re-sequencing (WGRS), QTL-seq, and bulk segregant RNA sequencing (BSR-seq), have played a pivotal role in advancing this field (Jaganathan et al. 2020).

Although RAD-seq, GBS, and WGRS have proven effective in identifying SNPs, QTL-seq, and BSR-seq offer distinct advantages. BSR-seq directly identifies candidate genes by sequencing the complete transcriptome of contrasting bulk samples, making it particularly valuable in scenarios involving large and intricate genomes, where sequencing costs remain a concern or a reference genome is absent (Jaganathan et al. 2020). Furthermore, QTL-seq integrates BSA with NGS methods, enabling more

efficient QTL mapping with relatively shorter intervals compared to other approaches, making it widely adopted in contemporary research.

In the present study, we employed QTL-seq analysis for two reasons. Firstly, cucumbers are a diploid species with 14 chromosomes and a genome size of approximately 367 Mb (Yang and Sagar 2022). Moreover, this species has a readily accessible reference genome. Additionally, we focused on mapping lines that exhibited responses to DM under field conditions. This suggests that alterations in the transcriptomes of these lines may extend beyond the effects attributed solely to DM-responses, and encompass other factors. These considerations guided our choice to utilize QTL-seq analysis, a method previously proven successful in a study conducted by Win et al. (2017).

Given the significance of the population type in QTL mapping, various mapping populations, including F_2, RIL, NIL, and double haploids (DH), have been employed for QTL mapping analyses (Varshney et al. 2019). Currently, both RIL and NIL are commonly used for the fine mapping of QTLs. While each of these populations has its own set of advantages and disadvantages, NIL is generally preferred because of its high genetic similarity within the population, except for the target genomic region. This characteristic enables the identification of narrower intervals, as shown in previous studies (Fridman et al. 2000; Jander et al. 2002; Uga et al. 2013; Song et al. 2015). Moreover, population size plays a crucial role in narrowing down target QTL regions. Initial QTL mapping typically involves 50–250 individuals or more, as suggested by Collard et al. (2005). To achieve a better resolution of QTL regions, it is essential to increase the number of individuals. Presently, the utilization of a large number of progenies, ranging from approximately 500 to over 10 000, is necessary to introduce a sufficient number of recombination events that can reduce the QTL regions to shorter genomic segments (Jaganathan et al. 2020). In our study, we employed RIL lines to fine-map *dm2.1* (4.19 Mb) and *dm2.*2 (1.94 Mb), successfully narrowing them down to 333 Kb and 296 Kb, respectively. For *dm5.1*, we effectively utilized NIL lines to reduce it from 8.5 Mb to 694 Kb. In this analysis, we employed 100, 131, and 146 individuals for *dm2.1*, *dm2.2*, and *dm5.1*, respectively, each showing signs of recombination. Our approach typically narrowed down these previously identified QTL regions to approximately 8–15% of their original size, with *dm2.1*, *dm2.2*, and *dm5.1* containing 31, 35, and 55 putative genes, respectively.

However, despite our efforts, these narrowed-down segments were still too large to identify specific DM-resistance candidate genes. Consequently, we applied an additional method, SNP-mining, to further refine these regions. Using this method, we successfully reduced the size of segments by identifying regions that exhibited 100% matched SNPs between the DM-R and DM-S parental lines and the R- and S-bulk samples. By applying SNP-mining, we ultimately narrowed down *dm2.1* to 62 Kb, *dm2.2* to 85 Kb, and *dm5.1* to 80 Kb. These refined regions encompassed seven, ten, and five putative genes, respectively.

By analyzing the sequence polymorphisms and examining the expression patterns of the narrowed-down regions, we identified three genes, *CsaV3_2G012920*, *CsaV3_2G030320*, and *CsaV3_5G015170* as potential candidates for controlling DM-resistance in *dm2.1*, *dm2.2*, and *dm5.1*, respectively. Among

these, *CsaV3_2G012920* encodes 1-aminocyclopropane-1-carboxylate oxidase (ACO), which plays a crucial role in regulating ethylene biosynthesis under specific conditions, such as flooding, tension wood formation, cotton fiber cell elongation, and fruit ripening (English et al. 1995; Vriezen et al. 1999; Andersson-Gunneras et al. 2003; Shi et al. 2006; Love et al. 2009; Van de Poel et al. 2012). Our 3D *in silico* modeling revealed that a single non-synonymous mutation ($I^{91} \rightarrow V^{91}$) in ACO did not significantly alter its structural conformation, except for the substitution of an amino acid in the α-helix domain. Notably, this mutation did not affect the conserved 2-His-1-carboxylate F (II)-binding motif, which is commonly found in all ACOs (Shaw et al. 1996). Moreover, the non-synonymous mutation ($I^{91} \rightarrow V^{91}$) did not overlap with other critical residues essential for ACO activity (Kadyrzhanova et al. 1999; Seo et al. 2004; Zhang et al. 2004; Brisson et al. 2012; Dilley et al. 2013).

The regulation of the *ACO* gene can occur at multiple levels, including transcriptional, post-transcriptional, or post-translational (Houben and Van de Poel 2019). Our findings strongly support the hypothesis that *ACO* expression is transcriptionally regulated in response to DM-infection, potentially leading to ET biosynthesis. The involvement of ET in plant resistance to biotic stress is well-established (Van der Ent and Pieterse 2012). Although ET has traditionally been associated with plant defense against necrotrophic pathogens, its role in biotrophic and hemibiotrophic pathogens has been less explored, in contrast to the well-documented involvement of salicylic acid (SA) in these types of pathogens (Glazebrook 2005; Boatwright and Pajerowska-Mukhtar 2013). However, a report suggested that ET enhances wheat resistance to the biotrophic pathogen *Blumeria graminis*, which causes powdery mildew (PM) (Zhang et al. 2019). Furthermore, ET treatment has been shown to enhance cucumber resistance to another PM-causing biotrophic pathogen *Podosphaera xanthii* (Zhang et al. 2022). Our data strongly support the involvement of ET in biotrophic DM-resistance in cucumber, akin to its role in PM-resistance in wheat and cucumber.

CsaV3_2G030320 (CsCA) encodes carbonic anhydrase (CA), an enzyme responsible for facilitating the conversion between CO_2 and HCO^{3-} (Meldrum and Roughton 1933). A substantial body of evidence supports the notion that plants regulate *CA* expression to adapt to challenging conditions, characterizing *CA* as a stress-responsive enzyme (DiMario et al. 2017; Floryszak-Wieczorek and Arasimowicz-Jelonek 2017; Rudenko et al. 2018, 2021). In our observations of the 3D structures of both CA predicted proteins, we found no significant structural differences, except for four amino acid substitutions ($F^{26} \rightarrow I^{26}$, $T^{165} \rightarrow I^{165}$, $G^{194} \rightarrow D^{194}$, and $D^{287} \rightarrow N^{287}$). These results suggest that these structural changes are unlikely to result in altered enzymatic activity of *CsCA*.

The role of *CA* expression in plant defense responses appears to be intricate. Some reports have indicated a decrease in *CA* expression during infections with pathogens such as *Plasmopara viticola* (grapevine DM) and *Phytophthora infestans* (potato late blight) (Restrepo et al. 2005, Polesani et al. 2008). Similarly, *CA* has also been shown to negatively regulate *Arabidopsis* immunity to *Pst* DC3000 (Wang et al. 2009). In contrast, *CA* expression increased in non-heading Chinese cabbage when infected with the DM pathogen *Hyaloperonospora parasitica*. Numerous studies have emphasized the positive

effect of *CA* on plant defense against various biotic stressors, including resistance to *Xanthomonas euvesicatoria* 85 − 10 in tomatoes, *Phytophthora infestans* in *Nicotiana benthamiana*, and *Pseudomonas syringae* in Arabidopsis (Restrepo et al. 2005; Zhou et al. 2019; Zhao et al. 2023).

Despite accumulating evidence of CA's involvement in plant immunity, little is known about its role in the molecular regulation of plant defense mechanisms. Recent studies have suggested a link between atmospheric CO_2 levels and plant defense responses, primarily through the regulation of stomatal closure (Melotto et al. 2008; Hu et al. 2010; Zhou et al. 2020). Stomata acts as entry points for many leaf pathogens and their closure can effectively prevent pathogen entry. It has been proposed that *CA* activation plays a role in stomatal closure during plant defense responses via an ABA-independent pathway (Majeau et al. 1994). Despite the well-established roles of SA and jasmonate (JA) in inducing stomatal closure during pathogen infection, there is conflicting evidence regarding whether *CA* responds to ET, although ET has been shown to inhibit ABA-induced stomatal closure in *Arabidopsis* (Yoko 2005; Chen and Gallie 2015). Moreover, although CA-mediated pathogen-induced stomatal closure has been suggested as a contributing factor to pathogen resistance, it may not be the sole determinant of pathogen resistance (Zhou et al. 2020). Nonetheless, our findings strongly support the notion that *CA* plays a beneficial role in resisting biotrophic pathogens, potentially under the positive regulation of ET.

CsaV3_5G015170 (*CsSTPK*) encodes a member of the PITSLRE protein kinase family, which constitutes serine/threonine protein kinases (STPK). PITSLRE kinases have been implicated in various biological processes in animals and humans, including RNA processing, transcriptional regulation, apoptosis induction, oncogenesis, and dopamine/glutamate signaling in animals and humans (Lahti et al. 1995; Knockaert et al. 2002; Trembley et al. 2004). However, information on PITSLRE kinases in plants is scarce. In *Arabidopsis*, the *cyclin-dependent Ser/Thr protein kinase* (*CDKG*) gene displayed similarity to the *PITSLRE protein kinase* gene found in animals and humans (Menges et al. 2005). *CDKG1* and *CDKG2* in *Arabidopsis* are involved in regulating recombination and synapsis during meiosis, as well as in activating adventitious root initiation (Zabicki et al. 2013; Nibau 2020).

Although direct evidence supporting the role of PITSLRE kinases in plant defense against biotic stress is currently lacking, we hypothesized that they may play a role in defense mechanisms, given their potential connection to apoptotic signaling pathways in animals and humans (Lahti et al. 1995). Our *in-silico* 3D protein structure analysis highlighted the structural differences in the C-terminal region (after the 653rd amino acid), which may be implicated in the activation of STPK-dependent defense signaling pathways. Considering the limited information available on *STPKs* in plants, these results suggest that further investigation into the role of *STPKs* in responding to biotrophic pathogens is warranted.

In our experiments involving the exogenous application of ET-releasing ETH, we observed that all three candidate genes associated with DM-resistance exhibited increased transcript levels after ETH treatment (Fig. 7). Additionally, the ETH treatment effectively prompted stomatal closure (Supplementary Fig. 5). Furthermore, when comparing the kinetics of stomatal action, it became evident that DM-resistance exhibited notably reduced stomatal conductance after 6 hour of ETH application (Fig. 8).

These observations strongly support the notion that the mechanism underlying DM-resistance is mediated by an ET-dependent signaling pathway. Based on these findings, we proposed a molecular model for DM-resistance, as illustrated in Fig. 9. When *P. cubensis* attempts to penetrate cucumber leaves, it initiates a defense response by activating *CsACO* expression, which, in turn, leads to the biosynthesis of ET. Elevated ET levels induce the expression of both *CsCA* and *CsSTPK*, which promote stomatal closure to hinder pathogenic hyphal entry and activate ET-mediated defense signaling, respectively.

Several studies have emphasized the intricate nature of DM-resistance genetics. This complexity is further illustrated by the distribution of DM-resistance QTLs, which include DM-resistance candidate genes, (Supplementary Fig. 9). Specifically, the role of *CsACO* as a key regulator controlling DM-resistance within *dm2.1* regions has been identified by various research groups (Wang et al. 2016, 2018; Win et al. 2017). Furthermore, *CsCA* was identified as a DM-resistance regulator within the *dm2.2* region identified by Win et al. (2017). However, it is noteworthy that the position of *dm2.2* identified by Wang et al. (2018) did not overlap with *CsCA* (Supplementary Fig. 9). Additionally, *CsSTPK* serves as a regulator of DM-resistance within the *dm5.1* regions recognized by several research groups (Supplementary Fig. 9; Bai et al. 2008; Win et al. 2017).

Declarations

Author contributions SL conceptualized the study. KTW and CYZ were responsible for the development of the plant material. MBA carried out fieldwork and genetic analysis. MBA and SB conducted the sequence data analysis. MBA and HL performed statistical analyses. SL and MBA wrote the manuscript. CW and TW reviewed the manuscript and provided the comments.

Acknowledgements This work was supported under the framework of the International Cooperation Program (NRF-2022K2A9A2A06037703) and the Basic Science Research Program (2020R1A2C108800 and RS-2023-00208020), managed by the National Research Foundation of Korea.

Conflict of interest statement The authors declare no conflicts of interest.

Compliance with ethical standards Not applicable to this study.

Data availability statement All whole-genome sequences were submitted to the Sequence Read Archive (SRA) database of the National Center for Biotechnology Information (NCBI) (https://www.ncbi.nlm.nih.gov/sra/term=) and can be accessed using the following IDs: dm2.1-F_7-R-bulk (SRR26038220), dm2.1-F_7-S-bulk (SRR26038219), dm2.2-F_7-R-bulk (SRR26038218), dm2.2-F_7-S-bulk (SRR26038217), dm5.1-BC_4F_2-R-bulk (SRR26038216), and dm5.1-BC_4F_2-S-bulk (SRR26038215).

Supplementary data Supplementary data is available at *Molecular Breeding* online.

References

1. Andersson-Gunneras S, Hellgren JM, Bjorklund S, Regan S, Moritz T, Sundberg B (2003) Asymmetric expression of a poplar ACC oxidase controls ethylene production during gravitational induction of tension wood. The Plant J 34(3):339-49.
2. Badri Anarjan M, Bae I, Lee S (2021) Marker-Assisted Evaluation of Two Powdery Mildew Resistance Candidate Genes in Korean Cucumber Inbred Lines. Agronomy 11, 2191.
3. Badri Anarjan M, Begum S, Bae I, Lee S (2023) Mutation in the *GA3ox* gene governs short-internode characteristic in a korean cucumber inbred line. Horticulture, Environment, and Biotechnology 64(3), pp.485-495.
4. Badri Anarjan M, Li H, Lee S (2024) Current Status of Viral Resistance Molecular Breeding in Cucumbers (*Cucumis sativus* L.). In Allele Mining for Genomic Designing of Vegetable Crops (pp. 105-131) CRC Press.
5. Bai Z, Yuan X, Cai R, Liu L, He H, Zhou H, Pan J (2008) QTL analysis of downy mildew resistance in cucumber. Prog Nat Sci 18:706-710.
6. Barnes WC, Epps WM (1954) An unreported type of resistance to cucumber downy mildew. Plant Dis Rep 38:620.
7. Berg JA, Hermans FW, Beenders F, Abedinpour H, Vriezen WH, Visser RG, Bai Y, Schouten HJ (2021) The amino acid permease (AAP) genes *CsAAP2A* and *SlAAP5A/B* are required for oomycete susceptibility in cucumber and tomato. Mol Plant Pathol 22:658–672.
8. Berg JA, Hermans FW, Beenders F, Lou L, Vriezen WH, Visser RG, Bai Y, Schouten HJ (2020) Analysis of QTL *DM4.1* for downy mildew resistance in cucumber reveals multiple subQTL: a novel RLK as candidate gene for the most important subQTL. Front Plant Sci 11:569876.
9. Boatwright JL, Pajerowska-Mukhtar K (2013) Salicylic acid: an old hormone up to new tricks. Mol Plant Pathol 14:623–34.
10. Brisson L, El Bakkali-Taheri N, Giorgi M, Fadel A, Kaizer J, Reglier M (2012) 1-Aminocyclopropane-1-carboxylic acid oxidase: insight into cofactor binding from experimental and theoretical studies. JBIC Journal of Biological Inorganic Chemistry 17, 939–949.
11. Call AD, Criswell AD, Wehner TC, Ando K, Grumet R (2012a) Resistance of cucumber cultivars to a new strain of cucurbit downy mildew. Hort Science 47:171-178.
12. Call AD, Criswell AD, Wehner TC, Klosinska U, Kozik EU (2012b) Screening cucumber for resistance to downy mildew caused by *Pseudoperonospora cubensis* (Berk. and Curt.) Rostov. Crop Sci 52:577-592.
13. Chen Z, Gallie DR (2015) Ethylene regulates energy-dependent non-photochemical quenching in *Arabidopsis* through repression of the xanthophyll cycle. PLOS One 10(12):e0144209.
14. Cobb JN, DeClerck G, Greenberg A, Clark R, McCouch S (2013) Next generation phenotyping: requirements and strategies for enhancing our understanding of genotype–phenotype relationships and its relevance to crop improvement. Theor Appl Genet 126:867–887.
15. Cohen Y, Rubin AE, Galperin M, Ploch S, Runge F, Thines M (2014) Seed transmission of *Pseudoperonospora cubensis*. PLOS One 9:e109766.

16. Cohen Y, Van den Langenberg KM, Wehner TC, Ojiambo PS, Hausbeck M, Quesada-Ocampo LM, Lebeda A, Sierotzki H, Gisi U (2015) Resurgence of *Pseudoperonospora cubensis*: The causal agent of cucurbit downy mildew. Phytopathol 105:998-1012.
17. Collard BC, Jahufer MZ, Brouwer JB, Pang EC (2005) An introduction to markers, quantitative trait loci (QTL) mapping and marker-assisted selection for crop improvement: the basic concepts. Euphytica 142:169–196.
18. Dilley DR, Wang Z, Kadirjan-Kalbach DK, Ververidis F, Beaudry R, Padmanabhan K (2013) 1-Aminocyclopropane-1-carboxylic acid oxidase reaction mechanism and putative post-translational activities of the *ACCO* protein. AoB Plants 1; 5:plt031.
19. DiMario RJ, Clayton H, Mukherjee A, Ludwig M, Moroney JV (2017) Plant carbonic anhydrases: structures, locations, evolution, and physiological roles. Mol Plant 10(1):30–46.
20. Dinka SJ, Campbell MA, Demers T, Raizada MN (2007) Predicting the size of the progeny mapping population required to positionally clone a gene. Genet 176:2035–2054.
21. English PJ, Lycett GW, Roberts JA, Jackson MB (1995) Increased 1-aminocyclopropane-1-carboxylic acid oxidase activity in shoots of flooded tomato plants raises ethylene production to physiologically active levels. Plant Physiol 1, 109(4):1435-40.
22. Floryszak-Wieczorek J, Arasimowicz-Jelonek M (2017) The multifunctional face of plant carbonic anhydrase. Plant Physiol Biochem112:362–368.
23. Fridman E, Pleban T, Zamir D (2000) A recombination hotspot delimits a wild-quantitative trait locus for tomato sugar to 484 bp within an invertase gene. Proceedings of the National Academy of Sciences of the United States of America 97:4718–4723.
24. Glazebrook J (2005) Contrasting mechanisms of defense against biotrophic and necrotrophic pathogens. Annu Rev Phytopathol 43:205–27.
25. He Y, Wei M, Yan Y, Yu C, Cheng S, Sun Y, Zhu X, Wei L, Wang H, Miao L (2022 0 Research advances in genetic mechanisms of major cucumber diseases resistance. Front Plant Sci 19, 13:862486.
26. Holmes GJ, Ojiambo PS, Hausbeck MK, Quesada-Ocampo L, Keinath AP (2015) Resurgence of cucurbit downy mildew in the United States: A watershed event for research and extension. Plant Dis 99:428-441.
27. Houben M, Van de Poel B (2019) 1-Aminocyclopropane-1-Carboxylic Acid Oxidase (ACO): The Enzyme That Makes the Plant Hormone Ethylene. Front Plant Sci 10:695.
28. Hu H, Boisson-Dernier A, Israelsson-Nordström M, Bohmer M, Xue S, Ries A, Godoski J, Kuhn JM, Schroeder JI (2010) Carbonic anhydrases are upstream regulators of CO2-controlled stomatal movements in guard cells. Nat Cell Biol 12:87–93.
29. Jaganathan D, Bohra A, Thudi M, Varshney RK (2020) Fine mapping and gene cloning in the post-NGS era: advances and prospects. Theor Appl Genet 133, 1791–1810.
30. Jander G, Norris SR, Rounsley SD (2002) Arabidopsis map-based cloning in the post-genome era. Plant Physiol 129:440–450.

31. Jenkins JM (1942) Downy mildew resistance in cucumbers. J Hered 33:35-38.
32. Kaçar YA, Simsek O, Solmaz I, Sari NE, Mendi YY (2012) Genetic diversity among melon accessions (*Cucumis melo*) from Turkey based on SSR markers. Genet Mol Res 11:4622–31.
33. Kadyrzhanova D, McCully TJ, Warner T, Vlachonasios K, Wang Z, Dilley DR (1999) Analysis of ACC Oxidase Activity by Site-Directed Mutagenesis of Conserved Amino Acid Residues, in Biology and Biotechnology of the Plant Hormone Ethylene II, eds A. K. Kanellis, (Dordrecht: Springer), 7–12.
34. Knockaert M, Greengard P, Meijer L (2002) Pharmacological inhibitors of cyclin-dependent kinases. Trends Pharmacol Sci 1, 23(9):417-25.
35. Lahti JM, Xiang J, Kidd VJ (1995) The PITSLRE protein kinase family. Prog Cell Cycle Res 1:329-38.
36. Li L, He H, Zou Z, Li Y (2018) QTL analysis for downy mildew resistance in cucumber inbred line PI197088. Plant Dis 102, 1240–1245.
37. Love J, Björklund S, Vahala J, Hertzberg M, Kangasjärvi J, Sundberg B (2009) Ethylene is an endogenous stimulator of cell division in the cambial meristem of Populus. PNAS 7,106(14):5984-9.
38. Lv J, Qi J, Shi Q, Shen D, Zhang S, Shao G, Li H, Sun Z, Weng Y, Shang Y, Gu X (2012) Genetic diversity and population structure of cucumber (*Cucumis sativus* L.). PLOS One e46919.
39. Majeau N, Arnoldo M, Coleman JR (1994) Modification of carbonic anhydrase activity by antisense and over-expression constructs in transgenic tobacco. Plant Mol Biol 25(3):377–385.
40. Meldrum NU, Roughton FJW (1933) Carbonic anhydrase. Its preparation and properties. Physiol J 80:113–142.
41. Melotto M, Underwood W, He SY (2008) Role of stomata in plant innate immunity and foliar bacterial diseases. Annu Rev Phytopathol 46:101–122.
42. Menges M, De Jager SM, Gruissem W, Murray JA (2005) Global analysis of the core cell cycle regulators of Arabidopsis identities novel genes, reveals multiple and highly specific profiles of expression and provides a coherent model for plant cycle control. The Plant Journal 41: 546- 566.
43. Nibau C, Lloyd A, Dadarou D, Betekhtin A, Tsilimigka F, Phillips DW, Doonan JH (2020) *CDKG1* is required for meiotic and somatic recombination intermediate processing in *Arabidopsis*. The Plant Cell 32:4, 1308–1322.
44. Ojiambo PS, Gent DH, Quesada-Ocampo LM, Hausbeck MK, Holmes GJ (2015) Epidemiology and population biology of *Pseudoperonospora cubensis*: A model system for management of downy mildews. Annu Rev Phytopathol 53:223-246.
45. Pan J, Tan J, Wang Y, Zheng X, Owens K, Li D, Li Y, Weng Y (2018) STAYGREEN (*CsSGR*) is a candidate for the anthracnose (*Colletotrichum orbiculare*) resistance locus *cla* in Gy14 cucumber. Theor Appl Genet 131:1577–1587.
46. Pang X, Zhou X, Wan H, Chen J (2013) QTL mapping of downy mildew resistance in an introgression line derived from interspecific hybridization between cucumber and *Cucumis hystrix*. J Phytopathol 161:536-543.

47. Polesani M, Desario F, Ferrarini A, Zamboni A, Pezzotti M, Kortekamp A, Polverari A (2008) cDNA-AFLP analysis of plant and pathogen genes expressed in grapevine infected with *Plasmopara viticola*. BMC Genomics 9:142.
48. Qi J, Liu X, Shen DI, Miao H, Xie B, Li X, Zeng P, Wang S, Shang Y, Gu X, Du Y (2013) A genomic variation map provides insights into the genetic basis of cucumber domestication and diversity. Nat Genet 45:1510–15.
49. Restrepo S, Myers KL, Del Pozo O, Martin GB, Hart AL, Buell CR, Fry WE, Smart CD (2005) Gene profiling of a compatible interaction between Phytophthora infestans and Solanum tuberosum suggests a role for carbonic anhydrase. Mol Plant-Microbe Interact 18, 913–922.
50. Rudenko N, Borisova-Mubarakshina NM, Ignatova MK, Fedorchuk LP, Nadeeva-Zhurikova TM, Ivanov B (2021) Role of Plant Carbonic Anhydrases under Stress Conditions. IntechOpen.
51. Rudenko NN, Ignatova LK, Zhurikova EM, Novichkova NS, Ivanov BN (2018) Plant carbonic anhydrases, their role in stress defense and possible practical use. J stress physiol biochem 14(1):27–38.
52. Rudus I, Sasiak M, Kępczynski J (2013) Regulation of ethylene biosynthesis at the level of 1-aminocyclopropane-1-carboxylate oxidase (ACO) gene. Acta Physiol Plant 35 295–307.
53. Seo YS, Yoo A, Jung J, Sung SK, Yang DR, Kim WT (2004) The active site and substrate-binding mode of 1-aminocyclopropane-1-carboxylate oxidase determined by site-directed mutagenesis and comparative modelling studies. Biochem J 380, 339–346.
54. Shaw J, Chou Y, Chang R, Yang SF (1996) Characterization of the ferrous ion binding sites of apple 1-aminocyclopropane-1-carboxylate oxidase by site-directed Mutagenesis. Biochem Biophys Res Commun 700, 697–700.
55. Shi YH, Zhu SW, Mao XZ, Feng JX, Qin YM, Zhang L, Cheng J, Wei LP, Wang ZY, Zhu YX (2006) Transcriptome profiling, molecular biological, and physiological studies reveal a major role for ethylene in cotton fiber cell elongation. The Plant Cell 1:18(3):651-64.
56. Sikdar B, Bhattacharya M, Mukherjee A, Banerjee A, Ghosh E, Ghosh B, Roy SC (2010) Genetic diversity in important members of the Cucurbitaceae using isozyme, RAPD, and ISSR markers. Biol Plant 54:135–40.
57. Song XJ, Kuroha T, Ayano M, Furuta T, Nagai K, Komeda N, Segami S, Miura K, Ogawa D, Kamura T, Suzuki T (2015) Rare allele of a previously unidentified histone H4 acetyltransferase enhances grain weight, yield, and plant biomass in rice. PNAS 112:76–81.
58. St. Amand PC, Wehner TC (1991) Crop loss to 14 diseases in cucumber in the North Carolina for 1983 to 1988. Cucurbit Genetics Cooperative Report 14:15–7.
59. Szczechura W, Staniaszek M, Klosinska U, Kozik EU (2015) Molecular analysis of new sources of resistance to *Pseudoperonospora cubensis* (Berk. et Curt.) Rostovzev in cucumber. Russ J Genet 51:974-979.
60. Takagi H, Abe A, Yoshida K, Kosugi S, Natsume S, Mitsuoka C, Uemura A, Utsushi H, Tamiru M, Takuno S, Innan H (2013) QTL-seq: rapid mapping of quantitative trait loci in rice by whole genome

re-sequencing of DNA from two bulked populations. The Plant J 74:174–183.

61. Tan J, Wang Y, Dymerski R, Wu Z, Weng Y (2022) *Sigma factor binding protein 1* (*CsSIB1*) is a putative candidate of the major-effect QTL *dm5.3* for downy mildew resistance in cucumber (*Cucumis sativus*). Theor Appl Genet 135, 4197–4215.
62. Trembley JH, Loyer P, Hu D, Li T, Grenet J, Lahti JM, Kidd VJ (2004) Cyclin Dependent Kinase 11 in RNA transcription and splicing. Progress in Nucleic Acid Research and Molecular Biology 77: 263–288.
63. Uga Y, Sugimoto K, Ogawa S (2013) Control of root system architecture by DEEPER ROOTING 1 increases rice yield under drought conditions. Nat Genet 45:1097–1102.
64. Van de Poel B, Bulens I, Markoula A, Hertog ML, Dreesen R, Wirtz M, Vandoninck S, Oppermann Y, Keulemans J, Hell R, Waelkens E (2012) Targeted systems biology profiling of tomato fruit reveals coordination of the Yang cycle and a distinct regulation of ethylene biosynthesis during postclimacteric ripening. Plant Physiol 1:160(3):1498-514.
65. Van der Ent S, Pieterse CMJ (2012) ETHYLENE: MULTI-TASKER IN PLANT-ATTACKER INTERACTIONS. In: McManus MT, ed. Plant Hormone Ethylene. New Jersey, USA: Wiley-Blackwell, 44. 343–77.
66. Varshney RK, Pandey MK, Bohra A (2019) Towards sequence-based breeding in legumes in post-genome sequencing era. Theor Appl Genet 132:797–816.
67. Vriezen WH, Hulzink R, Mariani C, Voesenek LA (1999) 1-Aminocyclopropane-1-carboxylate oxidase activity limits ethylene biosynthesis in *Rumex palustris* during submergence. Plant Physiol 1:121(1):189-96.
68. Wallace E, Adams M, Quesada-Ocampo LM (2015) First report of downy mildew on buffalo gourd (*Cucurbita foetidissima*) caused by *Pseudoperonospora cubensis* in North Carolina. Plant Dis 99:1861.
69. Wang Y, Tan J, Wu Z, VandenLangenberg K, Wehner TC, Wen C, Zheng X, Owens K, Thornton A, Bang HH, Hoeft E (2019) STAYGREEN, STAY HEALTHY: a loss-of-susceptibility mutation in the *STAYGREEN* gene provides durable, broad-spectrum disease resistances for over 50 years of US cucumber production. New Phytol 221, 415–430.
70. Wang Y, VandenLangenberg K, Wehner TC, Kraan PA, Suelmann J, Zheng X, Owens K, Weng Y (2016) QTL mapping for downy mildew resistance in cucumber inbred line WI7120 (PI330628). Theor Appl Genet 129:1493-1505.
71. Wang Y, VandenLangenberg K, Wen C, Wehner TC, Weng Y (2018) QTL mapping of downy and powdery mildew resistances in PI197088 cucumber with genotyping-by-sequencing in RIL population. Theor Appl Genet 131:597–611.
72. Wang YQ, Feechan A, Yun BW, Shafiei R, Hofmann A, Taylor P, Xue P, Yang FQ, Xie ZS, Pallas JA, Chu CC (2009) S-Nitrosylation of AtSABP3 antagonizes the expression of plant immunity. J Biol Chem 284:2131–2137.

73. Waterhouse A, Bertoni M, Bienert S, Studer G, Tauriello G, Gumienny R, Heer FT, de Beer TA, Rempfer C, Bordoli L, Lepore R (2018) SWISS-MODEL: homology modelling of protein structures and complexes. Nucleic Acids Res, 46:296–303.
74. Wehner TC, Shetty NV (1997) Downy mildew resistance of the cucumber germplasm collection in North Carolina field tests. Crop Sci 37:1331-1340.
75. Weng Y 2010 Genetic diversity among *Cucumis metuliferus* populations revealed by cucumber satellites. Hort Science 45:214–19.
76. Win KT, Vegas J, Zhang C, Song K, Lee S (2017) QTL mapping for downy mildew resistance in cucumber via bulked segregant analysis using next-generation sequencing and conventional methods. Theor Appl Genet 130:199-211.
77. Yang L, Sagar V, (2022) Genome Evaluation of Cucumber in Relation to Cucurbit Family. In: Pandey S, Weng Y, Behera TK, Bo K (eds) The Cucumber Genome. Compendium of Plant Genomes, Springer, Cham.
78. Yoko T (2005) Ethylene Inhibits Abscisic Acid-Induced Stomatal Closure in Arabidopsis. Plant Physiol, 138:4 2337–2343.
79. Yoshioka Y, Sakata Y, Sugiyama M, Fukino N (2014) Identification of quantitative trait loci for downy mildew resistance in cucumber (*Cucumis sativus* L.). Euphytica 198:265–276.
80. Żabicki P, Kuta E, Tuleja M, Rataj K, Malec P (2013) *Arabidopsis Cyclin-Dependent Kinase* Gene *CDKG;2* is Involved in Organogenic Responses Induced in Vitro. Acta Biologica Cracoviensia Series Botanica 55(1).
81. Zhang C, Badri Anarjan M, Win KT, Begum S, Lee S (2021) QTL-seq analysis of powdery mildew resistance in a Korean cucumber inbred line. Theor Appl Genet 134:435-51.
82. Zhang D, Wu S, Li N, Gao J, Liu S, Zhu S, Li Z, Ren G, Kuai B (2022) Chemical induction of leaf senescence and powdery mildew resistance involves ethylene-mediated chlorophyll degradation and ROS metabolism in cucumber. Hortic Res 17, 9:uhac101.
83. Zhang D, Zhu K, Dong L, Liang Y, Li G, Fang T, Guo G, Wu Q, Xie J, Chen Y, Lu P (2019) Wheat powdery mildew resistance gene Pm64 derived from wild emmer (*Triticum turgidum* var. *dicoccoides*) is tightly linked in repulsion with stripe rust resistance gene *Yr5*. Crop J 1, 7(6):761-70.
84. Zhang SP, Liu MM, Miao H, Zhang SQ, Yang YH, Xie BY, Wehner TC, Gu XF (2013) Chromosomal mapping and QTL analysis of resistance to downy mildew in *Cucumis sativus*. Plant Dis 97:245-251.
85. Zhang Z, Ren JS, Clifton IJ, Schofield CJ (2004) Crystal structure and mechanistic implications of 1-aminocyclopropane-1-carboxylic acid oxidase--the ethylene-forming enzyme. Chem Biol 11, 1383–1394.
86. Zhao J, Yuan Z, Han X, Bao T, Yang T, Liu Z, Liu H (2023) The Carbonic Anhydrase βCA1 Functions in POPW-Mediated Plant Defense Responses in Tomato. Int J Mol Sci 24, 11021.
87. Zhou Y, Van Leeuwen SK, Pieterse CM, Bakker PA, Van Wees SC (2019) Effect of atmospheric CO2 on plant defense against leaf and root pathogens of Arabidopsis. Eur J Plant Pathol 154:31–42.

88. Zhou Y, Vroegop-Vos IA, Van Dijken AJH (2020) Carbonic anhydrases CA1 and CA4 function in atmospheric CO_2-modulated disease resistance. Planta 251, 75.

Figures

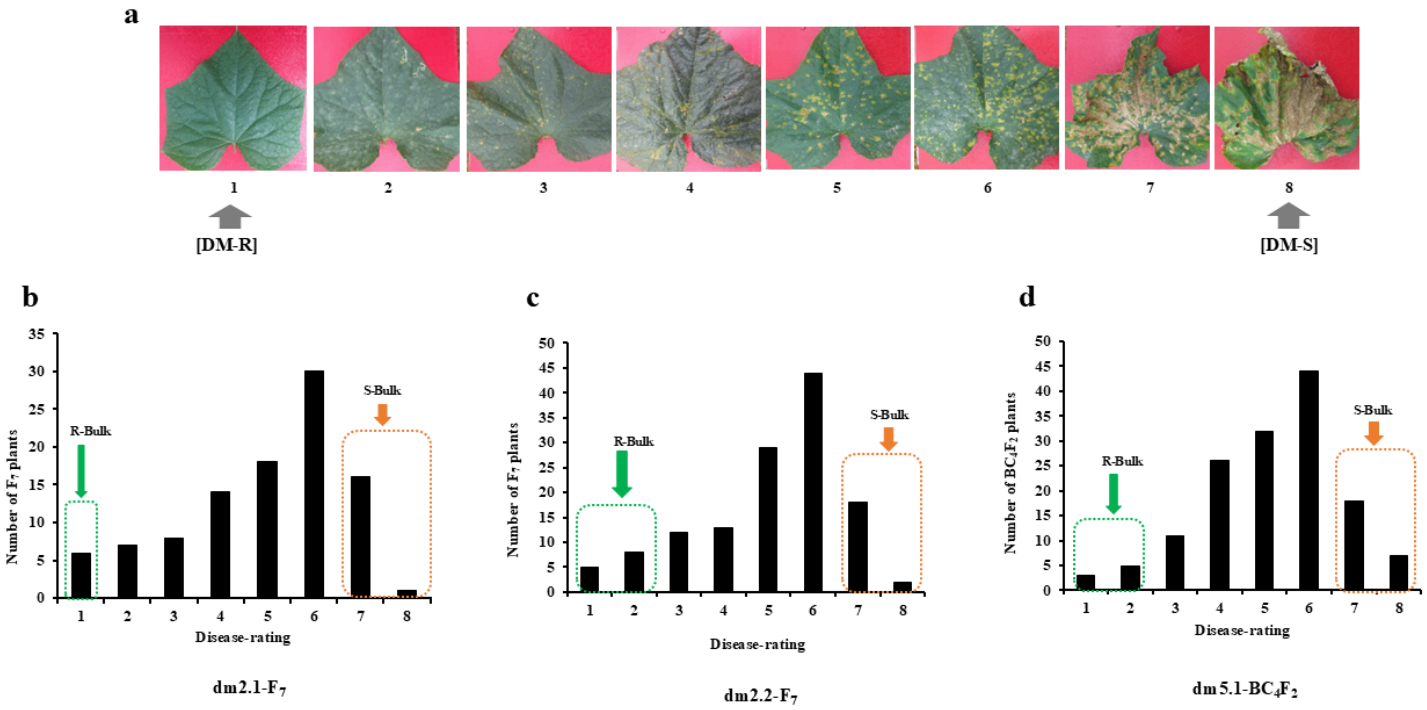

Figure 1

Various downy mildew (DM) disease symptoms and their distribution in mapping populations. Firstly, the DM-disease symptoms are categorized based on the disease index (DI) (**a**). These numbers shown in the figure correspond to the DI of DM, ranging from no disease symptoms (1) to the most severe symptoms (8). Next, the frequency distribution of DI within the dm2.1-F_7 (**b**), dm2.2-F_7 (**c**), and dm5.1-BC_4F_2 (**d**) populations is depicted. The DI values of the parental lines are indicated by gray arrows. Additionally, individuals exhibiting DM-resistance and susceptibility, which constituted the resistant and susceptible bulks, respectively, are marked with green and orange arrows. In graphs (**b**), (**c**), and (**d**), the X-axis represents the DI, while the Y-axis represents the number of individuals.

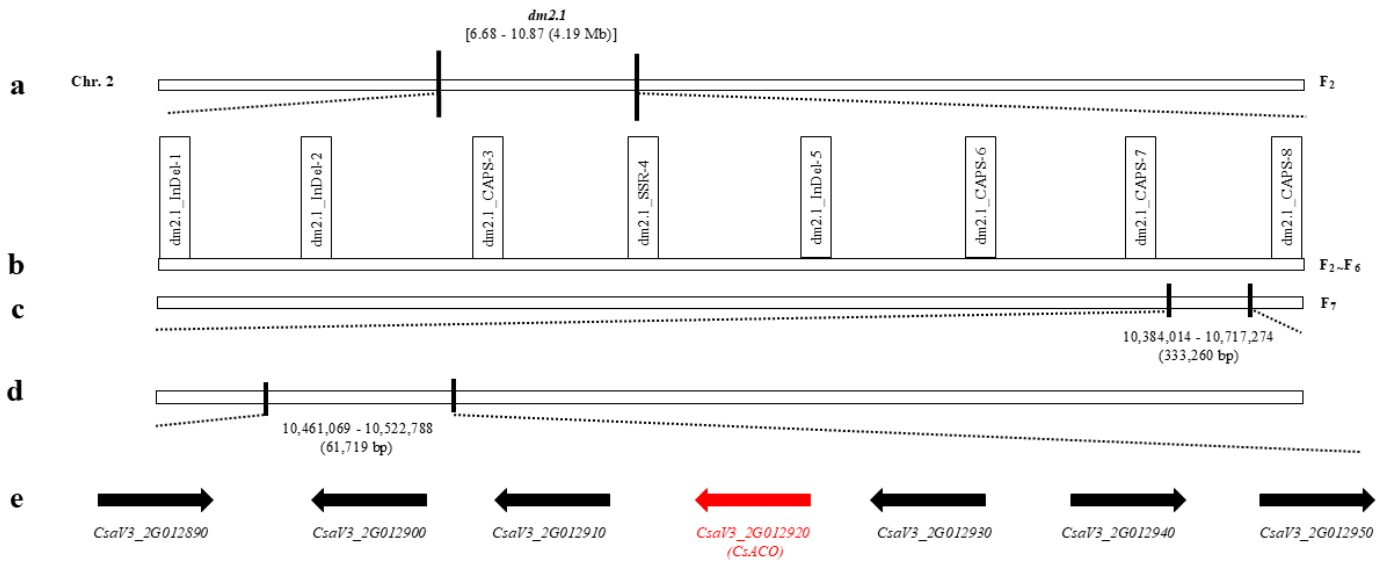

Figure 2

Enhancement of the *dm2.1* QTL associated with downy mildew (DM) resistance. Initially, the previously identified DM-resistance QTL (Win et al. 2017) was mapped to specific genomic position (**a**). Positions of markers using for developing of the RIL mapping population (**b**). Using QTL-seq analysis, this QTL region was then precisely refined into chromosomal segment, denoted by its corresponding size measurement (**c**). Further refinement was achieved through single nucleotide polymorphism (SNP)-mining, resulting in more precise intervals within this region (**d**). The genes within this refined QTL was annotated and visually represented as arrow bars. Notably, DM-resistance candidate gene is highlighted in red, and the direction of the arrow bars indicates the transcriptional direction of these genes (**e**). For detailed markers, physical positions, and gene list information for *dm2.1* major-effect DM-resistance QTL, refer Table 2 and Supplementary Table 1, 4.

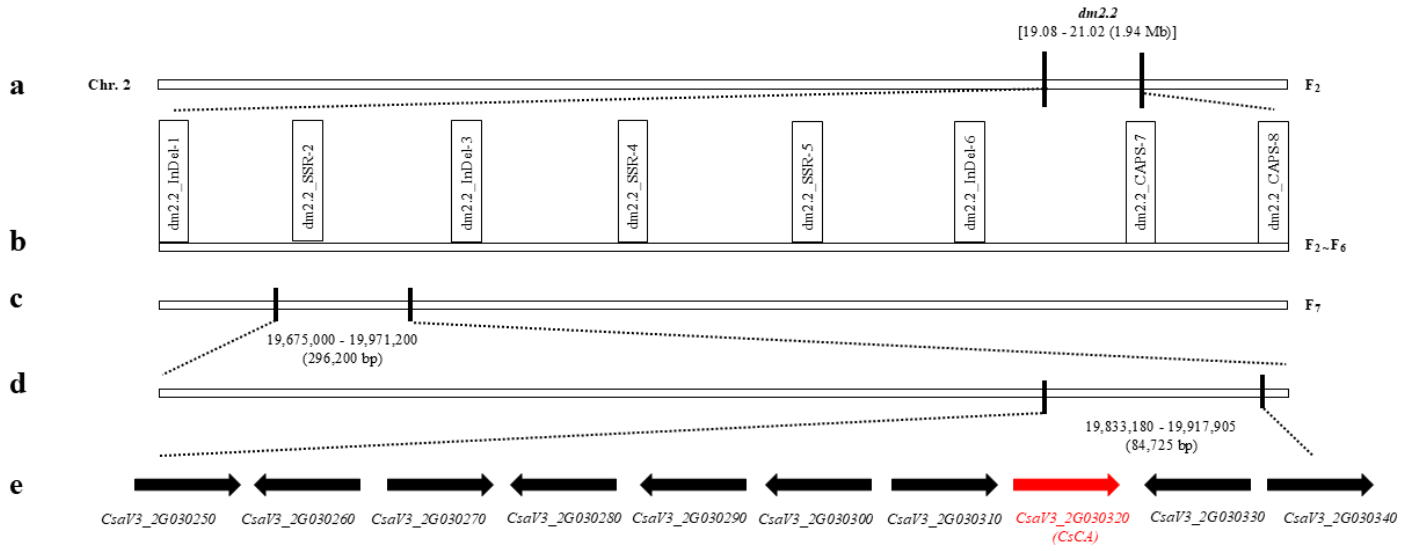

Figure 3

Enhancement of the *dm2.2* QTL associated with downy mildew (DM) resistance. Initially, the previously identified DM-resistance QTL (Win et al. 2017) was mapped to specific genomic position (**a**). Positions of markers using for developing of the RIL mapping population (**b**). Using QTL-seq analysis, this QTL region was then precisely refined into chromosomal segment, denoted by its corresponding size measurement (**c**). Further refinement was achieved through single nucleotide polymorphism (SNP)-mining, resulting in more precise intervals within this region (**d**). The genes within this refined QTL was annotated and visually represented as arrow bars. Notably, DM-resistance candidate gene is highlighted in red, and the direction of the arrow bars indicates the transcriptional direction of these genes (**e**). For detailed markers, physical positions, and gene list information for *dm2.2* major-effect DM-resistance QTL, refer Table 2 and Supplementary Table 1, 4.

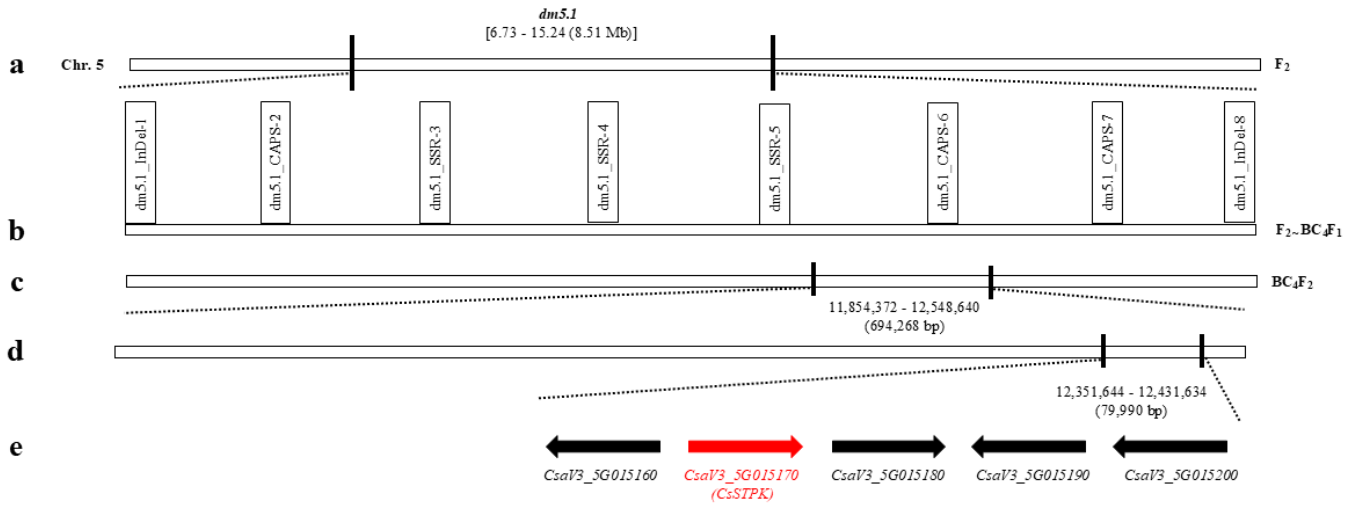

Figure 4

Enhancement of the *dm5.1* QTL associated with downy mildew (DM) resistance. Initially, the previously identified DM-resistance QTL (Win et al. 2017) was mapped to specific genomic position (**a**). Positions of markers using for developing of the NIL mapping population (**b**). Using QTL-seq analysis, this QTL region was then precisely refined into chromosomal segment, denoted by its corresponding size measurement (**c**). Further refinement was achieved through single nucleotide polymorphism (SNP)-mining, resulting in more precise intervals within this region (**d**). The genes within this refined QTL was annotated and visually represented as arrow bars. Notably, DM-resistance candidate gene is highlighted in red, and the direction of the arrow bars indicates the transcriptional direction of these genes (**e**). For detailed markers, physical positions, and gene list information for *dm5.1* major-effect DM-resistance QTL, refer Table 2 and Supplementary Table 1, 4.

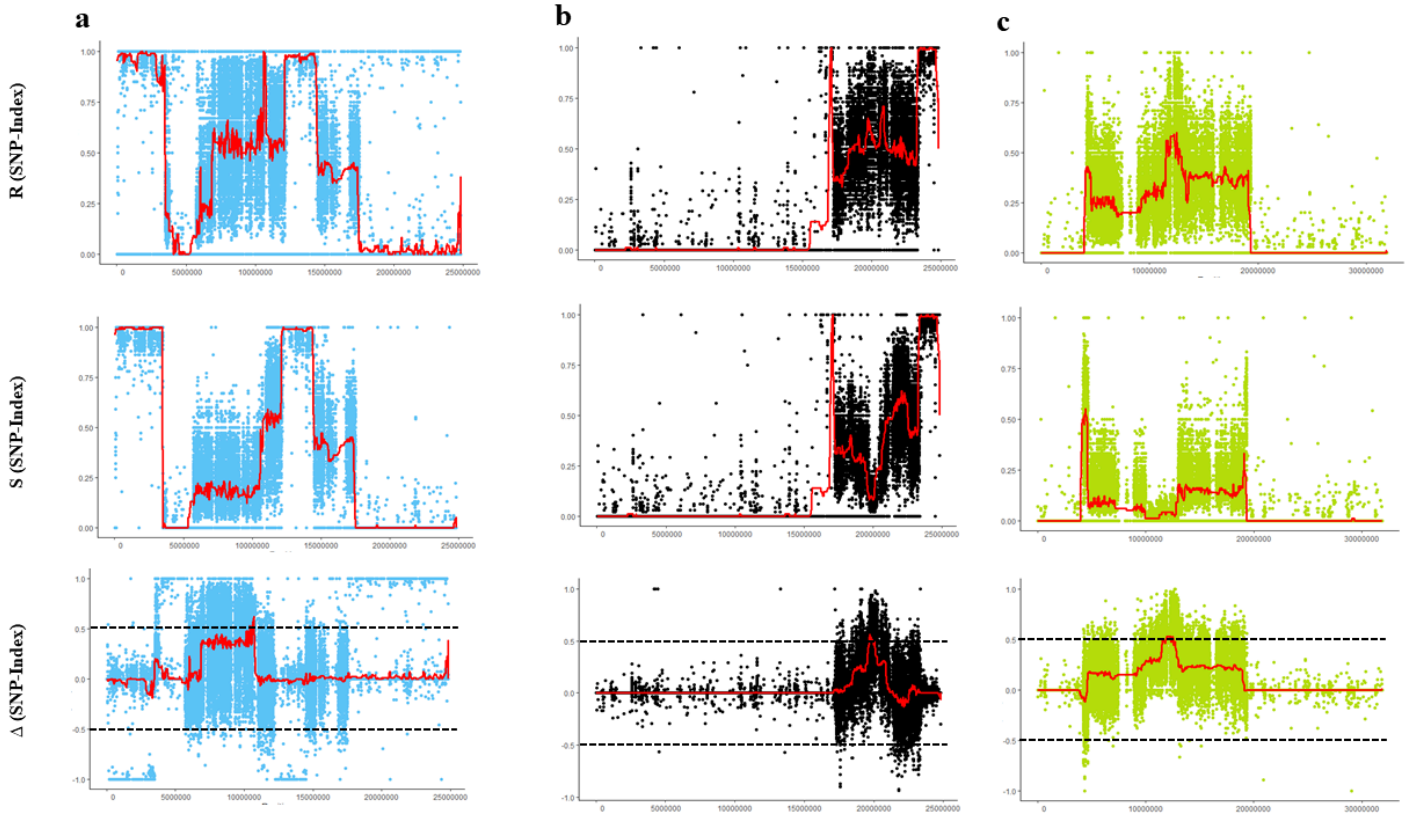

Figure 5

Enhancement of the quantitative trait locus (QTL) *dm2.1* (**a**), *dm2.2* (**b**), and *dm5.*1 (**c**) through QTL-seq analysis. The single nucleotide polymorphism (SNP)-index graphs were generated for both resistant (R) and susceptible (S) individuals. Additionally, a Δ (SNP-index) graph was plotted. These graphs were constructed by performing a QTL-seq analysis on the dm2.1-F_7, dm2.2-F_7, and dm5.1- BC_4F_2 populations to refine the *dm2.1*, *dm2.2*, and *dm5.1* QTLs. In these graphs, the X-axis represents the positions on chromosomes, while the Y-axis represents the SNP-index. The SNP-index was calculated using 10-km sliding windows and 2-Mb intervals. To establish a statistical confidence interval, the Δ (SNP-index) graphs were plotted under the null hypothesis of no QTLs ($P < 0.05$). The SNP-index values close to 1 in the resistant bulk (R-bulk) graph and close to 0 in the susceptible bulk (S-bulk) graph were employed to identify and define the *dm2.1*, *dm2.2*, and *dm5.1* QTLs.

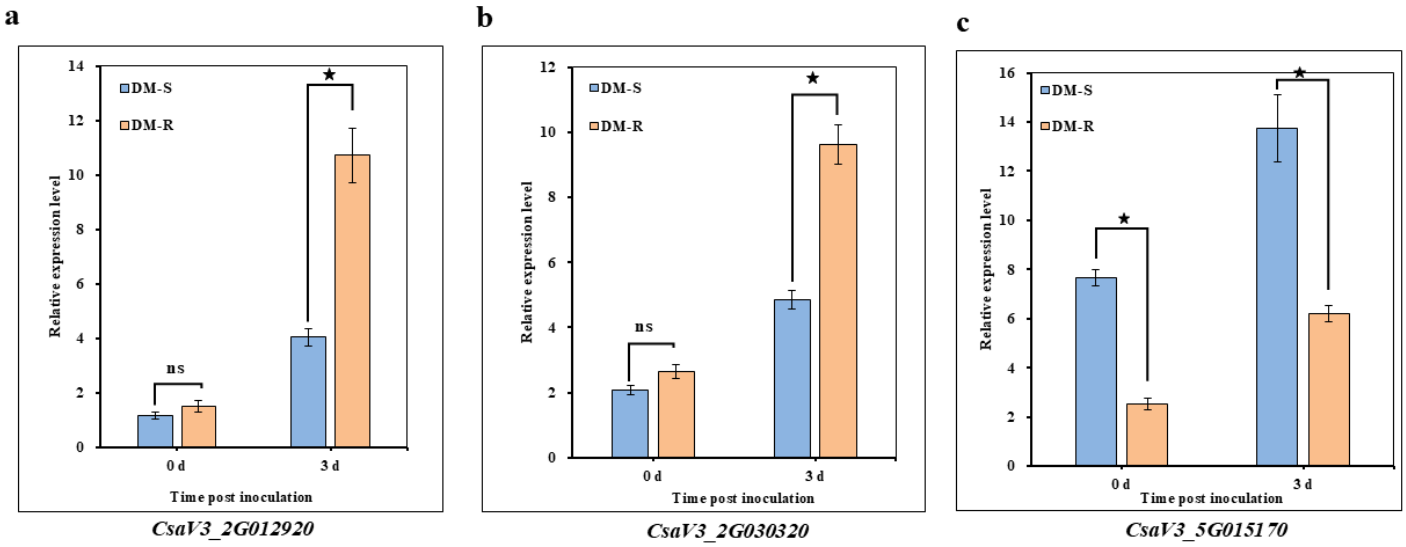

Figure 6

Expression profiles of downy mildew (DM) resistance candidate genes. The expression profiles of three candidate genes *CsaV3_2G012920*(**a**), *CsaV3_2G030320*(**b**), and *CsaV3_5G015170*(**c**) associated with the regulation of DM-resistance in quantitative trait loci (QTLs) *dm2.1*, *dm2.2*, and *dm5.1*, respectively. Gene expression analysis was conducted on cucumber leaves from WMEJ (DM-S) and TH118FLM (DM-R) plants at two distinct time points: 0 and 3 days post-inoculation (dpi). In the bar graph, the blue bars represent DM-S cucumbers, while the orange bars represent DM-R cucumbers. The graph displays the relative expression levels of the three candidate genes, with error bars indicating mean +/- standard error (n=3). Significantly different expression levels are indicated by asterisks ($P < 0.05$), which represents the *P*-value derived from a t-test, signifying observed variations in gene expression.

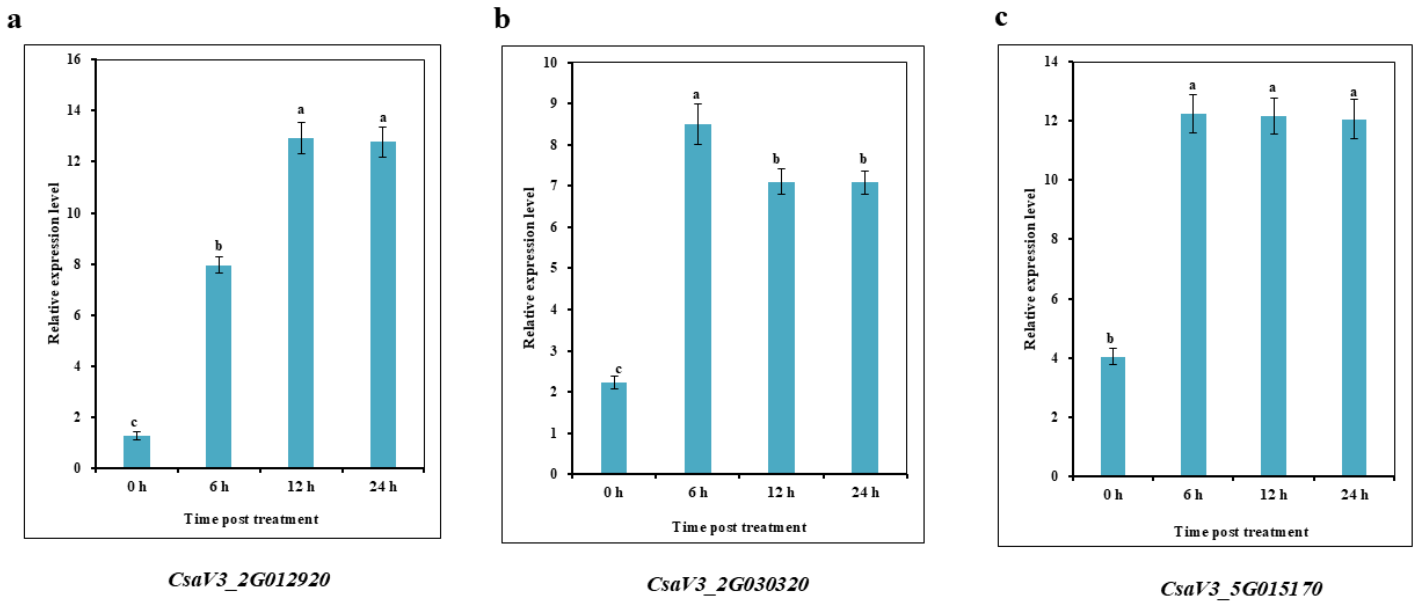

Figure 7

Analysis of downy mildew (DM) resistance candidate gene expression in response to ethephon (ETH) treatment. The transcriptional expression of three DM-resistance candidate genes *CsaV3_2G012920*(**a**), *CsaV3_2G030320*(**b**), and *CsaV3_5G015170*(**c**) was determined at four distinct time points: 0, 6, 12, and 24 hour post-treatment. The bar chart depicts the relative expression levels of these candidate genes, with error bars representing the mean +/- standard error (n=3). Statistically significant differences in gene expression are denoted by different letters ($P < 0.05$), highlighting the observed variations in gene expression in response to ETH treatment.

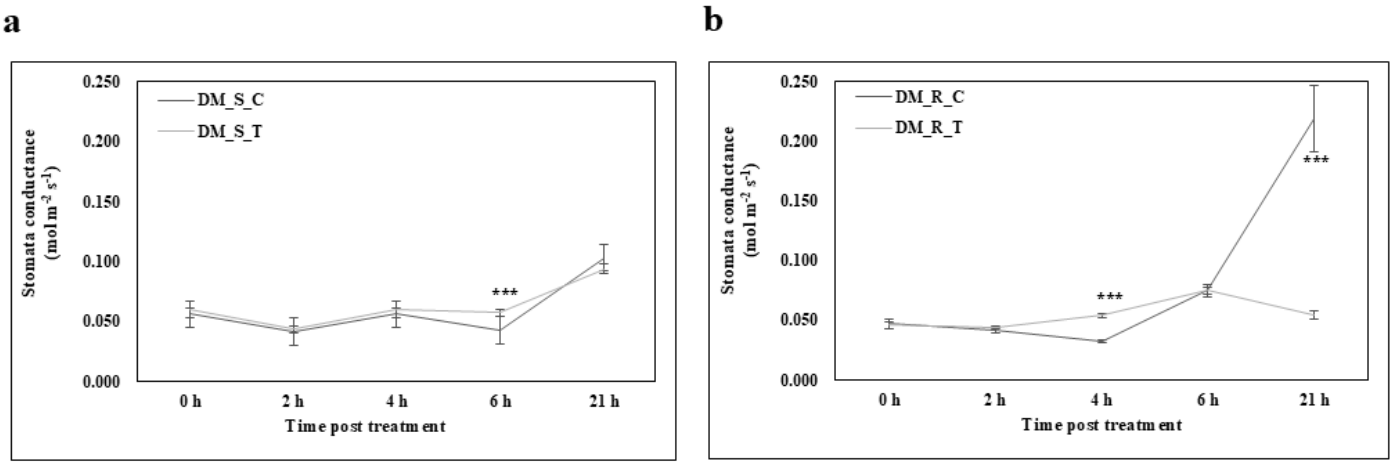

Figure 8

The comparison of stomatal conductance between DM-R (resistant) and DM-S (susceptible) plants under ethephon (ETH) application. The x-axis illustrates time intervals (0, 2, 4, 6, and 21 hours) following ETH and control solution application, while the y-axis represents stomatal conductance (mol m^{-2} s^{-1}). The black and gray bar graphs respectively display the stomatal conductance of control- (C) and ETH-treated (T) plants. The stomatal conductance data for DM-S and DM-R are respectively presented as (**a**) and (**b**). Asterisks indicate the significance levels denoted as *** ($p < 0.001$), reflecting differences. Each data point represents the mean and standard error derived from triplicate measurements.

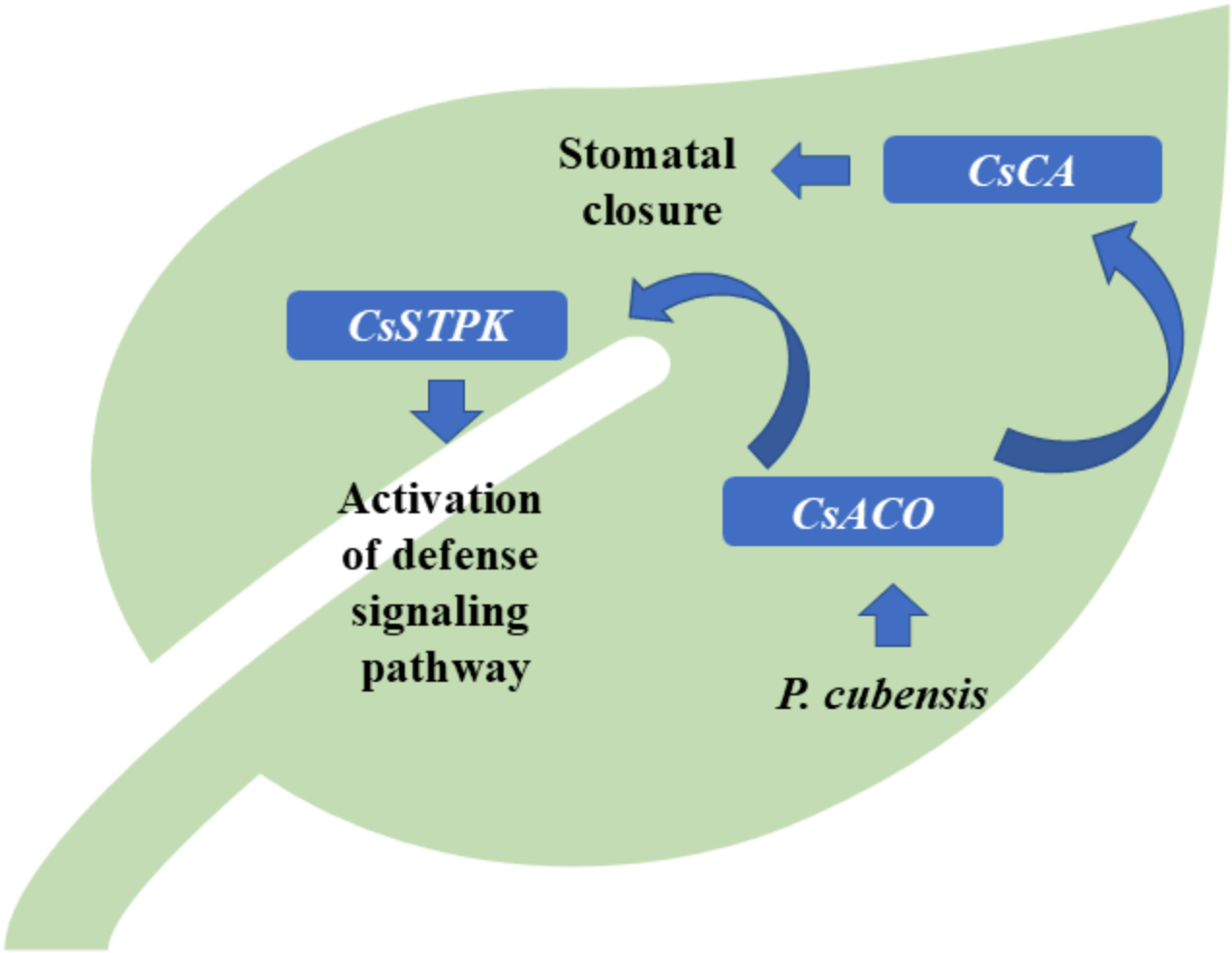

Figure 9

Model of downy mildew (DM) resistance in cucumber. Detection of the presence of the DM-causing *Pseudoperonospora cubensis* in cucumber leads to an increase in the mRNA transcripts of *CsACO*, which, in turn, enhances the biosynthesis of ethylene (ET). As ET levels rise, the mRNA transcripts of *CsCA*begin to accumulate, resulting in the closure of stomata to prevent the entry of pathogenic hyphae.

Concurrently, the expression of *CsSTPK* is activated, which initiates the ET-mediated defense signaling pathway in coordination with these events.

Supplementary Files

This is a list of supplementary files associated with this preprint. Click to download.

- DMSupplementaryData.docx